

DOI: 10.1016/S1872-5813(21)60084-1

Preparation of Ni-Fe alloy foam for oxygen evolution reaction

YANG Xiao-meng¹, LI Zuo-peng^{1,*}, QIN Jun¹, WU Mei-xia¹, LIU Jia-li¹, GUO Yong¹,
MA Yan-qing^{2,*}, FENG Feng^{1,*}

(1. School of Chemistry and Chemical Engineering, Shanxi Datong University, Datong 037009, China;

2. Tianjin International Center for Nanoparticles and Nanosystems, Tianjin University, Tianjin 300072, China)

Abstract: NiFe oxyhydroxide and hydroxide have been proven to be efficient and earth-abundant non-noble metal catalysts for the oxygen evolution reaction (OER). However, the fragile nature of these oxyhydroxides or hydroxides severely reduces the long-term stability and hinders the industrial applications. Meanwhile, the poor electrical conductivity of these materials also has seriously led to the higher overpotential when applying to the OER. Herein, a novel method using polyurethane (PU) sponge as electroplating was carried out to design NiFe alloy foam with different Fe content for OER. The physical properties of NiFe alloy foams were characterized by Scanning Electronic Microscopy (SEM), Energy Dispersive System (EDS) and X-Ray Diffraction (XRD), respectively, suggesting that the porous NiFe alloy is formed with uniform distribution of Ni and Fe. The OER performance was tested by Cyclic Voltammetry (CV), Linear Sweep Voltammetry (LSV), Electrochemical Impedance Spectroscopy (EIS), *I-t*, etc. The results showed that the doped Fe could significantly improve the conductivity and OER performance of Ni foam. The NiFe alloy foam with 30% Fe exhibited 292 mV overpotential at 10 mA/cm² and the Tafel slope 126.12 mV/decade in alkaline solution with excellent long-term stability. Without any complex electrode preparation processes and binders, NiFe alloy foam is much convenient to use as anode of water splitting in alkaline media for industrial applications.

Key words: OER; NiFe alloy foam; porous structure; water splitting

CLC number: O643.36; TQ116.2

Document code: A

With the rapid growth of sustainable energy such as wind and solar power, it becomes more and more important to utilize renewable energy more efficiently and stably. Electrochemical splitting water into hydrogen driven by renewable wind and solar energy provides an environmentally-friendly, carbon free and sustainable pathway to meet the ever-increasing energy demand^[1-3]. However, since the anode oxygen evolution reaction (OER) involves four consecutive proton coupling electron transfer reactions and oxygen-oxygen bond formation processes, the reaction is slow and needs higher positive voltage, which greatly hinders large-scale water electrolysis^[4-6]. Hence, the crucial challenge is how to reduce the overpotential of OER, and figuring out this issue by employing catalyst is a feasible approach. So far, the state-of-the-art OER catalyst both in alkaline and acidic solutions is IrO₂, which is located on the top of the volcano plot due to its excellent activity and stability. However, IrO₂ still suffers a considerable OER overpotential, meanwhile, the wide utilization of IrO₂ is hindered by its high cost and rare abundance on the earth^[7-9]. Therefore, it is

highly desirable to design cost-effective catalysts for water splitting by using non-noble metals.

Up to now, various low-cost alternatives have been investigated to catalyze OER, including metal oxides^[10-12], hydroxides^[13,14], chalcogenides^[15,16], phosphate^[17] and perovskites^[18,19]. However, further improvement is needed in terms of activity, stability and cost. Recently, 3d-transition metal (oxy)hydroxides have received tremendous attention due to many advantages such as earth abundance, low-cost and high catalytic activity^[13,14,20]. Among these catalysts, Fe-doped Ni (oxy)hydroxides are the most active electrocatalysts known for the oxygen evolution reaction in alkaline electrolytes, more efficient than pure NiOOH or Ni(OH)₂^[21]. However, the poor electrical conductivity of these materials has seriously led to the higher overpotential when applying to the commercial electrochemical splitting water. Meanwhile, the problem of long term stability urgently need to be solved. In order to improve the intrinsic conductivity of electrocatalysts, NiFe alloy catalysts for OER were developed. For example, some groups developed FeNi

Received: 2020-11-17; Revised: 2021-01-01

* Corresponding author. Tel & Fax: +86-352-7158185, E-mail: lizuopeng@126.com, mayanqing@tju.edu.cn, feng-feng64@263.net.

The project was supported by Natural Science Foundation of Shanxi (201701D121016, 201901D111310), the Science and Technology Innovation Project of Shanxi Province University (2020L0478) and Natural Science Foundation of Datong (201819, 2019160).

本文的英文电子版由 Elsevier 出版社在 ScienceDirect 上出版 (<http://www.sciencedirect.com/science/journal/18725813>)

alloy nanosphere embedded in carbon materials or nitrogen-doped nanocarbon hybrid catalysts with highly active and low-cost for oxygen evolution reaction. Lyu et al^[22] reported that FeNi₃@NC is more catalytically active than the same system covered by three N-doped carbon layers from density functional theory (DFT) calculations. Ma et al^[23] synthesized FeNi/NiFe₂O₄@NC hollow microcubes from bimetal MOFs which exhibited excellent electrocatalytic performances toward OER in alkaline media. Although the NiFe alloy/carbon materials composite catalysts exhibit excellent electrocatalytic performance toward OER, it is inevitable that a binder will be used to construct electrode, which may deteriorate conductivity and stability of the fabricated electrode, further affect the catalytic activity of electrocatalysts, especially for industrial applications. In this work, we developed a synthetic strategy of NiFe alloy foam for OER, which was much more convenient for water splitting in alkaline media for industrial applications due to the absence of binders and any complex electrode preparation processes.

1 Experimental

1.1 Preparation of NiFe alloy foam

The Ni-Fe alloy foam was prepared via co-electrodeposition method and removal of template

method according to the literature^[30]. As shown in Figure 1, the polyurethane sponge (2 mm thick) used as the electrodeposition template was firstly purified with a 0.1 mol/L KMnO₄ and 0.1 mol/L H₂SO₄, respectively. Then it was immersed in a reducing solution of 0.5 mol/L oxalic acid for 30 min, finally washed with deionized water for three times. Electroless plating was used to treat the conductive sponge. The composition of the applied plating solution was NiSO₄·6H₂O (25 g/L), Na₄P₂O₇·10H₂O (50 g/L), NaH₂PO₂·H₂O (25 g/L), and water with a pH value of 10.0–11.0. The plating reaction was conducted at 30 °C for 30 min. Electrodeposition of Ni-Fe alloy on treated organic foam was conducted with constant current electrolysis (~400 A/m²). The specific composition of the applied plating electrolyte solution was FeSO₄·7H₂O + NiSO₄·6H₂O (300 g/L), NaCl (8 g/L), H₃BO₃ (30 g/L), Na₂SO₄ (60 g/L) and MgSO₄ (50 g/L). The pH value of the plating solution was 5.0–5.5, and the plating temperature was 25 °C. The Ni:Fe ratio of Ni-Fe alloy can be adjusted according to the change of FeSO₄·7H₂O and NiSO₄·6H₂O. After electroplating for 1.0–2.0 h, a bright and metallic porous Ni-Fe alloy was obtained. Then, the porous Ni-Fe alloy was placed in an air oven at 600 °C for 4 min to remove the organic foam. Then the product was subjected to the reductive sintering at 850 °C for 40 min under a reductive atmosphere of NH₃.

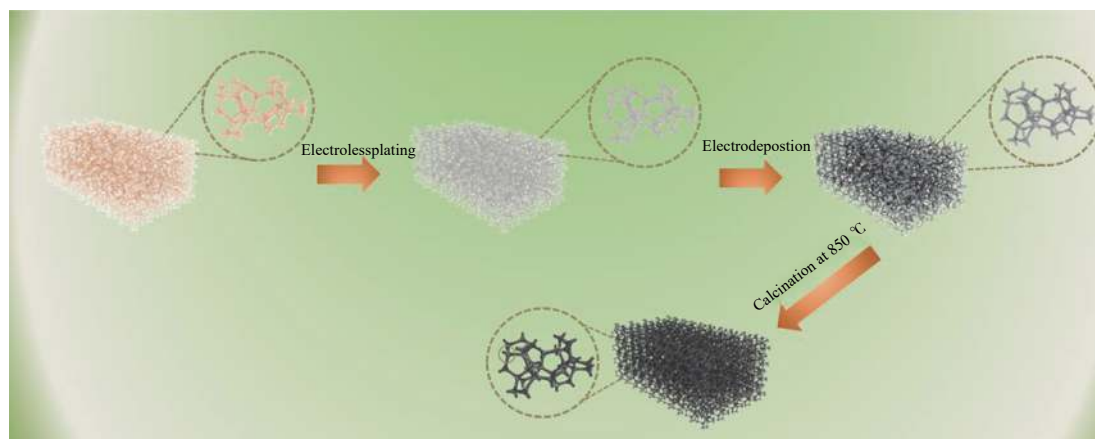


Figure 1 Synthesis process for NiFe alloy foam

1.2 Physical measurements

The morphology and elemental mapping of the prepared samples were observed by scanning electron microscopy (SEM) (TESCAN MAIA3, Czech) coupled with energy-dispersive X-ray spectroscopy (EDX), which was operated at an accelerating voltage of 3.0 kV. The compositions of the as-prepared samples were analyzed by inductively coupled plasma analysis (ICP Varian 720). X-ray powder diffraction (XRD) was performed using a Bruker D8-advance X-ray

diffractometer with graphite-monochromatized Cu K α radiation.

1.3 Electrochemical measurements

Electrochemical measurements were performed on a CHI760E electrochemical workstation (CH Instruments, Inc., Shanghai) in a standard three-electrode system, using NiFe alloy foam (0.25 cm²) as working electrode. Before the OER performance test, the electrode was soaked in 0.5 mol/L HCl solution for 5 min, then rinsed with deionized water, and dried. A

Pt foil electrode (1 cm^2) and an Ag/AgCl electrode were served as the counter and reference electrode, respectively. In all measurements, the Ag/AgCl reference electrode was calibrated with respect to reversible hydrogen electrode (RHE) according to $E(\text{RHE}) = E(\text{Ag}/\text{AgCl}) + 0.204 + 0.059\text{pH}$ in 1.0 mol/L KOH . The overpotential (η) was calculated by $E(\text{RHE}) - 1.23\text{V}$. Linear sweep voltammetry (LSV) measurements were conducted in the electrolyte at scan rate of 5 mV/s . $I-t$ curve was recorded at $+0.443\text{V}$ (vs RHE) for 4000 min. Electrochemical impedance

spectroscopy (EIS) measurements were performed on Zahner electrochemical workstation (Cimps-2, Germany) by applying an AC voltage of 10 mV amplitude in a frequency range from 0.01 Hz to 100 kHz at 1.50 V (vs RHE).

2 Results and discussion

All samples were firstly compared in appearance. As shown in Figure 2, the prepared Ni-Fe alloy foam showed gray color and metallic luster, and the color of samples gradually turned dark with the increase of Fe content from 0 to 100%.

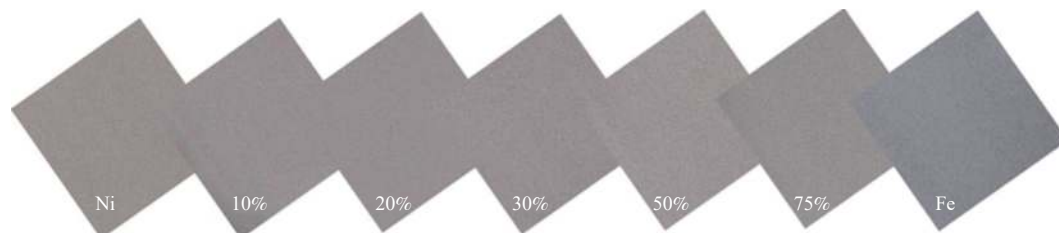


Figure 2 Morphology of Ni-Fe alloy foam with different Fe content

The influence of different Fe content on morphology is further investigated by SEM. Figure 3(a) shows the surface microstructure of pure nickel foam, which is relatively smooth and no impurities, and seems to be somewhat different to that of NiFe alloy foam. Figure 3(b)–(f) display the detailed morphology characteristics of Ni-Fe alloy foam with various Fe content at higher magnification. It is noteworthy that Fe content has great impact on the morphology of NiFe alloy foam. As shown in Figure 3(b)–(c), SEM micrographs of NiFe alloy foam with low Fe content (20% and 30%) exhibit much uneven and crude surface opening to the environment, which is like rolling hills in the range from 200 nm to $1 \mu\text{m}$. Meanwhile, crude surface is believed to provide an increased specific surface area, which plays a key role to improve electrocatalytic properties. When elevating Fe content, the crude surface disappears, as seen in Figure 3(d)–(e). Comparing with pure Ni or NiFe alloy foam, the surface of pure Fe foam has quiet difference morphology, which is very rough and irregular, and a large part of the surface shows many cracks, resembling the shape of burned charcoal, indicating that the crystallinity of pure Fe is very low, as shown in Figure 3(f). Figure 3(a')–(f') display 3d cross-linked skeleton of NiFe alloy foam at a lower magnification, which is expected to allow the efficient contact between catalysts and electrolyte and facilitate the easy release of generated O_2 gas during OER activity. Especially for the Figure 3(b)–(c) of NiFe alloy foam

with low Fe content, crude and uniform surface clearly increases the working area, which can further elevate the catalytic activity for OER.

The morphology of Ni-Fe alloy foam with 30% Fe content is further analyzed concretely by SEM with different magnification illustrated in Figure 4(a)–(c). There are some fine particles in Figure 4(a)–(b) decorated on the surface of the three-dimensional reticulated structure (Figure 4(c)), which can be attributed to the aggregation of Ni-Fe deposition. In addition, the composition of the certain point on Ni-Fe alloy foam is demonstrated by EDS displayed in Figure 4(e)–(g), and two elements, Ni and Fe, are detected in EDS spectrum. Meanwhile, it is clear that the ratio of Ni/Fe trends to be consistent in randomly selected spectrum 1 and spectrum 2, indicating that the Fe and Ni elements of the sample are uniformly distributed on the surface. This result can also be confirmed by element mapping. It can be seen from Figure 4(d) that Fe is distributed loosely on polyurethane sponge while nickel is distributed closely. The reason is that the content of Ni in the NiFe alloy is 70%, which is twice than the iron content. Therefore, the distribution of Ni and Fe elements on the entire structure is relatively uniform. For oxygen element, because the exposed area of corners of the structure is relatively large compared with other places, part of Ni and Fe elements are oxidized during the pretreatment, resulting in a dense distribution of oxygen element here.

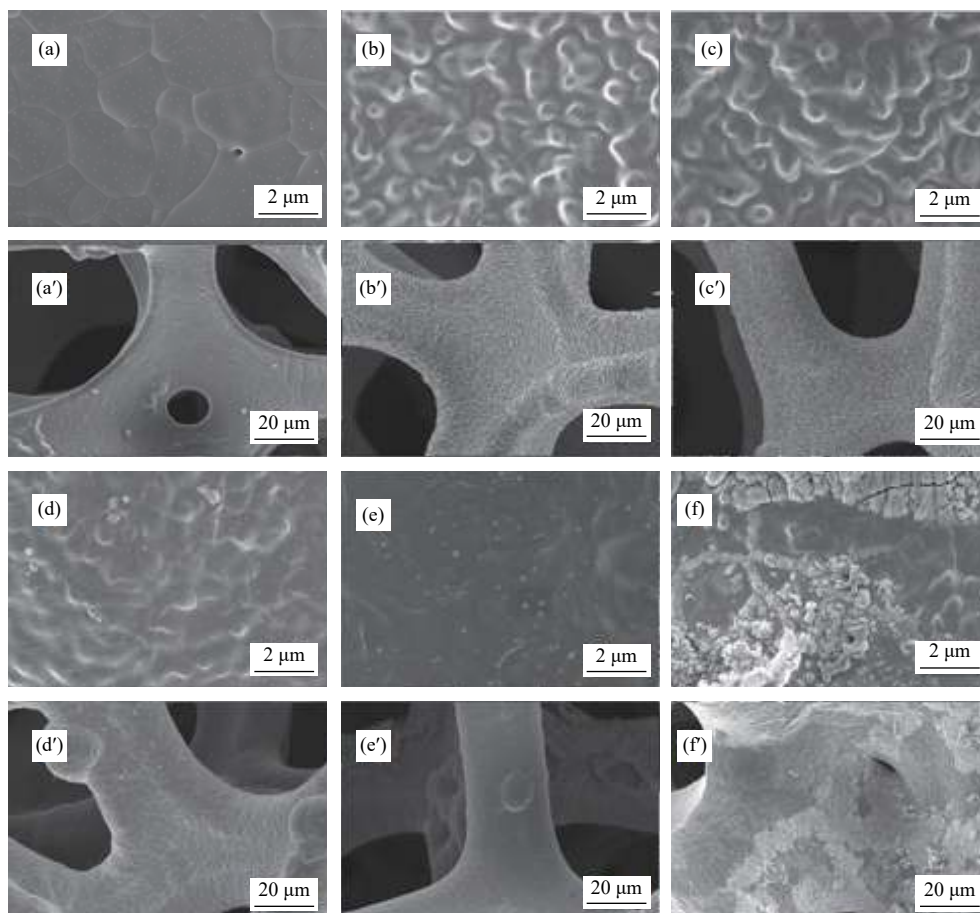


Figure 3 Scanning electron microscopy (SEM) micrograph for pure Ni and NiFe alloy foam with different Fe content (20%, 30%, 50%, 75%, 100%) at different magnification (2 μm and 20 μm)

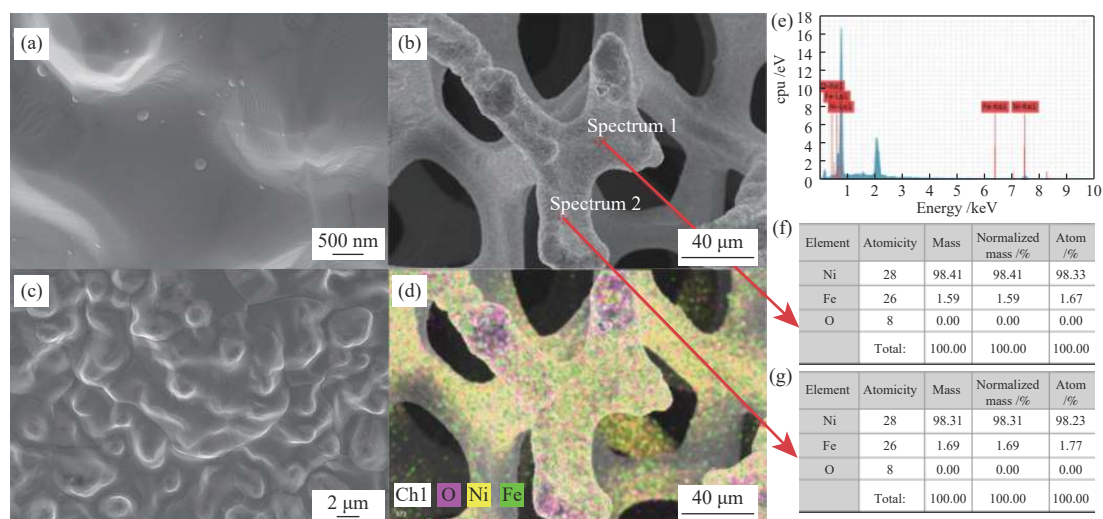


Figure 4 SEM((a)–(c)), mapping (d) and EDS((e)–(g)) for NiFe alloy foam with 30% Fe content

XRD contributed to analyzing all samples to obtain related information and thereby confirm the crystalline phases. As shown in Figure 5, there are two distinct diffraction peaks in pure iron, one of which at 44.7° is intense, the other at 64.9° is weak, corresponding to (110) and (200) crystal planes of Iron, respectively. Otherwise, no Fe peak appears on the

catalysts with different Fe content, suggesting that Fe has been alloyed with Ni. There are three obviously sharp diffraction peaks located at 44.5° , 51.8° and 76.4° for NiFe alloy foam, corresponding to (111), (200) and (220) crystal planes of the face-centered cubic (fcc) phase of Ni_3Fe , which is in agreement with SEM mapping, and further confirms the formation of Ni_3Fe

in NiFe alloy foam^[24, 31]. Further, it is observed that as Fe content increases from 10% to 75%, intensity of (111), (220) and (200) decreases, indicating that the crystallinity decreases^[25].

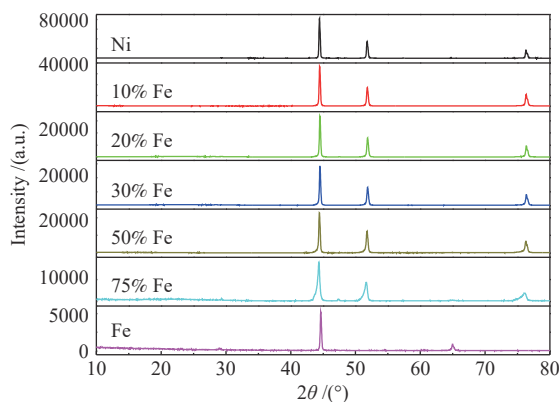


Figure 5 XRD patterns of Ni-Fe alloy foam with different Fe content

The electrocatalytic performance of all the catalysts was evaluated in 1 mol/L NaOH aqueous solution with a three-electrode system. Figure 6(a) shows the LSV curves of the NiFe alloys without any treatment. It is observed that except pure Fe, all catalysts shows an oxidation peak at around (1.35–1.45) V, by which we speculate that the Ni-Fe alloy may be oxidized during reaction, which means that the Ni-Fe alloy is one of the actual active sites of OER^[23, 26]. When the current density is 10 mA/cm², the corresponding overpotentials of pure Ni, pure Fe, Ni-Fe alloy with 10%, 20%, 30%, 50%, 75% Fe are 450, 493, 395, 407, 405, 400, and 560 mV, respectively. It can be seen that the NiFe alloy catalyst with 10% Fe content exhibits the highest catalytic activity. This result shows that the incorporating Fe has a positive impact on improving the electrocatalytic OER performance. The Tafel plots derived from LSV curves are exhibited in Figure 6(b), and the corresponding Tafel slopes are 217.03, 142.26, 114.55, 121.06, 139.96, 126.88, and 137.03 mV/decade, respectively. The slope value of the Ni-Fe alloy with 10% Fe content (114.55 mV/decade) is slightly lower than that of the other catalysts, demonstrating an effective catalytic kinetics for OER^[27]. In order to further improve their catalytic performance, the NiFe alloys were pre-treated with 0.5 mol/L hydrochloric acid. The LSV curves of the pre-treated NiFe alloys are shown in Figure 6(c). When the current density is 10 mA/cm², the corresponding overpotentials of pure Ni, pure Fe, 10%, 20%, 30%, 50%, 75% are 446, 400, 325, 339, 292, 505, and 348 mV, respectively. It can be seen that the catalyst with 30% Fe content exhibits the

highest catalytic activity by comparison. Meanwhile, the OER activity of the catalyst with 30% Fe content pre-treated with hydrochloric acid is much higher than that of the catalyst with 10% Fe content without any pretreatment, indicating that a certain concentration of hydrochloric acid plays a very important role in improving the electrocatalytic performance of the NiFe alloy. In the past, we also used other dilute acid such as sulfuric acid and nitric acid as treatment reagent for Ni-Fe alloy, but they are failed to improve the electrocatalytic performance. It can be conjectured that some complex containing Cl⁻ could be formed on the NiFe alloys, which can reduce the overpotential of the OER. The corresponding Tafel slopes of the NiFe alloys are 334.18, 187, 137.07, 187.98, 126.12, 155.63, and 159.87 mV/decade, respectively. It can be clearly seen that the NiFe alloy with 30% Fe content has the lowest Tafel slope (126.12 mV/decade), indicating the favorable OER kinetics^[28], and this result is in agreement with the result of LSV curves.

The CV curves (Figure 7(a)) of NiFe alloy foam with 30% Fe content were recorded at different scan rates in non-faradic region. The electrochemical active surface area of the sample is directly proportional to the double layer capacitance (C_{dl})^[29]. Combining the slope calculated from the linear relationship (Figure 7(b)), C_{dl} of NiFe alloy foam with 30% Fe content is highest, indicating that Ni-Fe alloy foam with 30% Fe content has a higher surface roughness, so more active sites are exposed and the electrocatalytic activity is enhanced. As shown in Figure 7(c), EIS of NiFe alloy foam with different Fe content was tested to further study the conductivity. The charge transfer (R_{ct}) of NiFe alloy foam with 30% Fe (1.08 $\Omega \cdot \text{cm}^2$) is the smallest compared with that of other Ni-Fe alloy foam, which can ensure a much faster charge transfer on the interface between the catalyst based electrode and electrolyte, resulting in the favorable electrocatalytic performance. This result can be attributed to the appropriate Fe-doping, which can change the carrier concentration and thus is beneficial to improving conductivity^[29]. Finally, the stability of the catalyst is very important for practical application of water splitting, and evaluated by amperometric I-t test in 1 mol/L NaOH aqueous solution. As displayed in Figure 7(d), within 700 min, the current density remains basically horizontal. Moreover, as the activation time increases, it shows an upward trend, proving that the catalyst has favorable stability. Therefore, NiFe alloy foam with 30% Fe content could be considered as a promising OER catalyst for practical application.

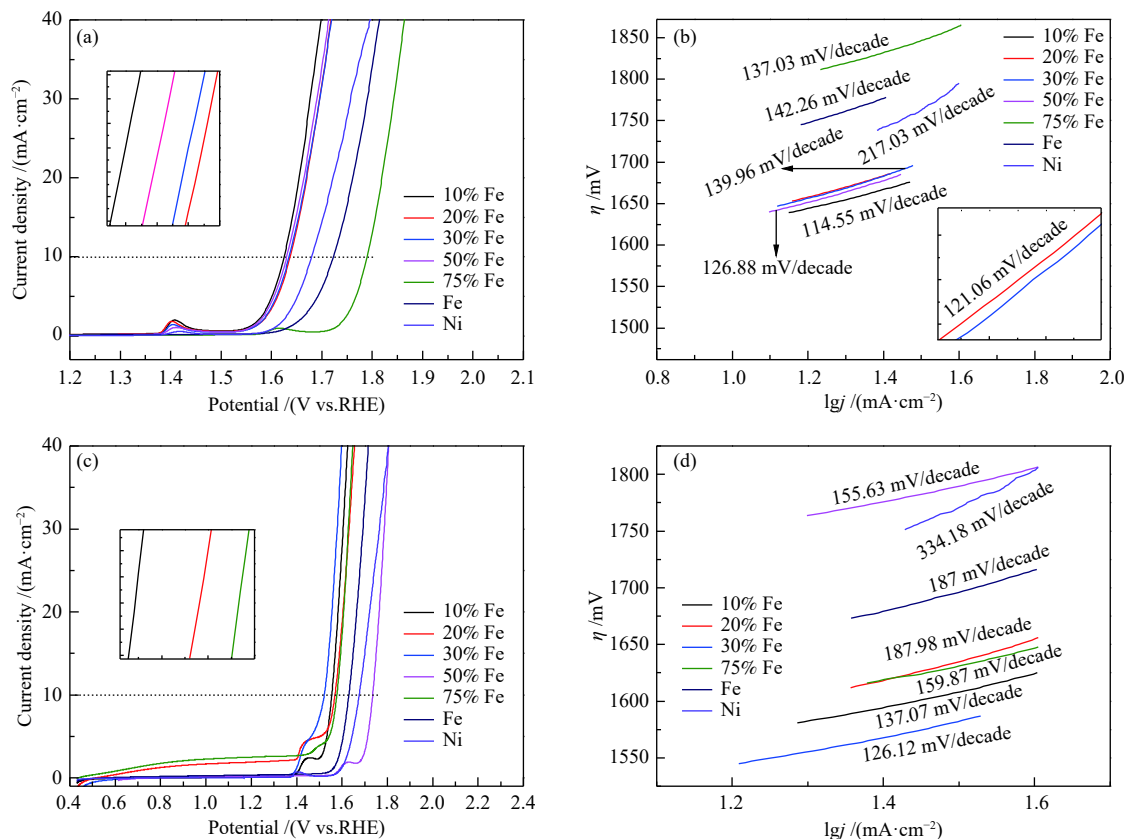


Figure 6 LSV curves ((a), (c)) and their Tafel curves ((b), (d)) of NiFe alloy foam with varied Fe content and pure Ni

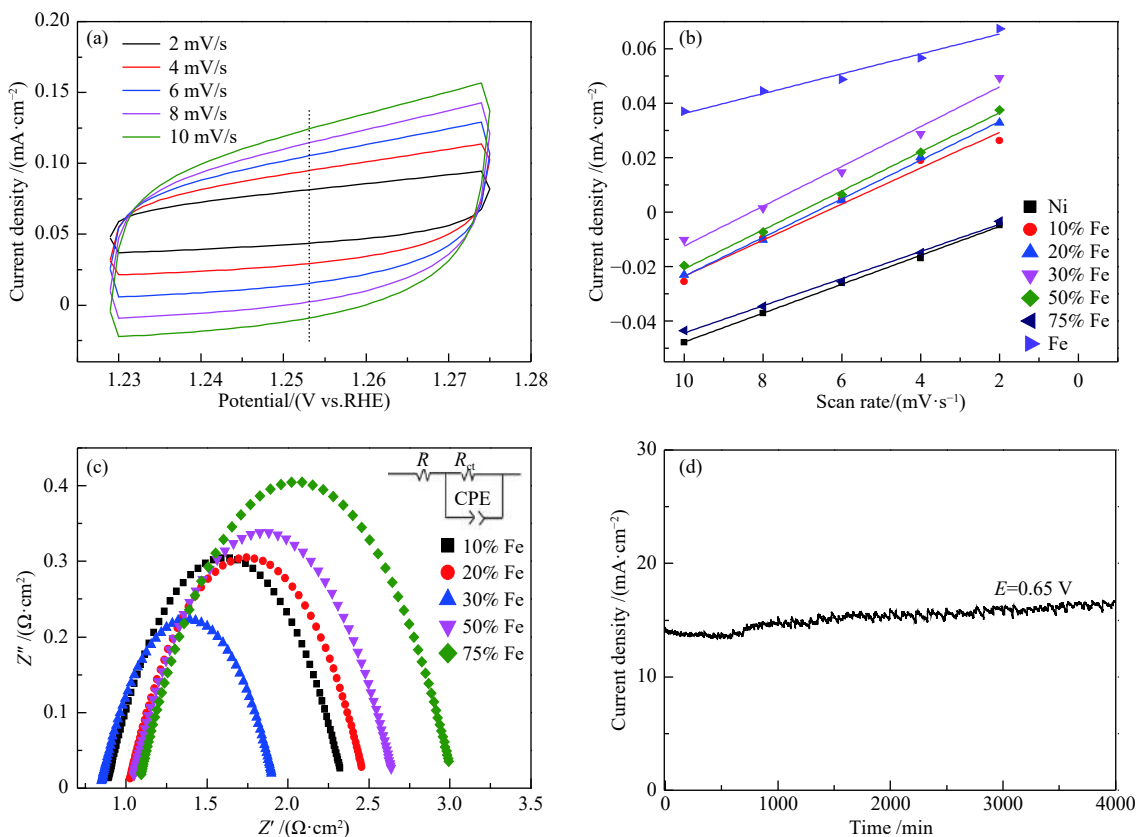


Figure 7 CVs of NiFe alloy foam with 30% Fe content at different scan rate (a); Linear fitting of the capacitance currents versus CVs scan rates (b); EIS of Ni-Fe alloy foam with varied Fe content (c); $I-t$ curves of Ni-Fe alloy foam with 30% Fe content at 0.443V(vs.RHE)(d)

3 Conclusions

In summary, a series of NiFe alloy foams with different Fe content were successfully prepared, and their surface morphology, element content, XRD pattern properties were studied in detail. By optimizing the constitution of the NiFe alloy foams, the best performance with overpotential 292 mV at $j = 10 \text{ mA/cm}^2$ and robust durability was achieved. This behaviour may be ascribed to the unique structure with three-dimensional reticulated structure with low Fe

content. Meanwhile, EIS spectrum and C_{dl} test show that the NiFe alloy foams with 30% Fe content has excellent electron transfer ability and more active sites, which also prove that it has the best OER performance. Without any complex electrode prepared processes and binders, NiFe alloy foam is much convenient to use as anode of water splitting in alkaline media for industrial applications. Our study could offer an important strategy to fabricate OER electrocatalysts with highly activity, low cost and simple way .

References

- [1] ZENG K, ZHANG D. Recent progress in alkaline water electrolysis for hydrogen production and applications[J]. *Prog Energy Combust*, 2010, **36**(3): 307–326.
- [2] FENG L, YU G T, WU Y Y, LI G D, LI H, SUN Y H, ASEFA T, CHEN W, ZOU X X. High-index faceted Ni_3S_2 nanosheet arrays as highly active and ultrastable electrocatalysts for water splitting[J]. *J Am Chem Soc*, 2015, **137**(44): 14023–14026.
- [3] GU Y, CHEN S, REN J, JIA Y A, CHRN C M, KOMARNENI S, YANG D J, YAO X D. Electronic structure tuning in $\text{Ni}_3\text{FeN/r-GO}$ aerogel toward bifunctional electrocatalyst for overall water splitting[J]. *ACS Nano*, 2018, **12**(1): 245–253.
- [4] KOPER M T M. Hydrogen electrocatalysis: a basic solution[J]. *Nat Chem*, 2013, **5**: 255–256.
- [5] ZHENG Y, JIAO Y, ZHU Y, CAI Q, VASILEFF A, LI L H, HAN Y, CHEN Y, QIAO S Z. Molecule-level $g\text{-C}_3\text{N}_4$ coordinated transition metals as a new class of electrocatalysts for oxygen electrode reactions[J]. *J Am Chem Soc*, 2017, **139**(9): 3336–3339.
- [6] WU M, GUO B, NIE A, LIU R. Tailored architectures of FeNi alloy embedded in N-doped carbon as bifunctional oxygen electrocatalyst for rechargeable zinc-air battery[J]. *J Colloid Interface Sci*, 2020, **561**: 585–592.
- [7] PETKUCHEVA E, BORISOV G, LEFTEREFTEROVA E, HEISS J, SCHNAKENBERG U, SLAVCHEVA E. Gold-supported magnetron sputtered Ir thin films as OER catalysts for cost-efficient water electrolysis[J]. *Int J Hydrog Energy*, 2018, **43**(35): 16905–16912.
- [8] FORGIE R, BUGOSH G, NEYERLIN K C, LIU Z, STRASSER P. Bimetallic Ru electrocatalysts for the oer and electrolytic water splitting in acidic media[J]. *Electrochem Solid-State Lett*, 2010, **13**(4): B36–B39.
- [9] NONG H N, GAN L, WILLINGER E, TESCHNER D, STRASSER P. IrO_x core-shell nanocatalysts for cost- and energy-efficient electrochemical water splitting[J]. *Chem Sci*, 2014, **5**(8): 2955–2963.
- [10] GAO W, XIA Z, CAO F, HO J C, JIANG Z, QU Y. Comprehensive understanding of the spatial configurations of CeO_2 in NiO for the electrocatalytic oxygen evolution reaction: Embedded or surface-loaded[J]. *Adv Funct Mater*, 2018, **28**(11): 1706056.
- [11] JIN H, WANG J, SU D, WEI Z, PANG Z, WANG Y. In situ cobalt-cobalt oxide/N-doped carbon hybrids as superior bifunctional electrocatalysts for hydrogen and oxygen evolution[J]. *J Am Chem Soc*, 2015, **137**(7): 2688–2694.
- [12] PICKRAHN K L, PARK S W, GORLIN Y, LEE H B R, JARAMILLO T F, BENT S F. Active MnO_x electrocatalysts prepared by atomic layer deposition for oxygen evolution and oxygen reduction reactions[J]. *Adv Eng Mater*, 2012, **2**(10): 1269–1277.
- [13] ZHAO Z, LAMOUREUX P S, KULKARNI A, BAJDICH M. Trends in oxygen electrocatalysis of 3d-Layered (oxy)(hydro)oxides[J]. *Chem Electro Chem*, 2019, **11**(15): 3423–3431.
- [14] QIN Y, WANG F, SHANG J, IQBAL M, HAN A, SUN X, XU H, LIU J. Ternary NiCoFe-layered double hydroxide hollow polyhedrons as highly efficient electrocatalysts for oxygen evolution reaction[J]. *J Energy Chem*, 2020, **43**: 104–107.
- [15] MAJHI K C, KARFA P, MADHURI R. Bimetallic transition metal chalcogenide nanowire array: An effective catalyst for overall water splitting[J]. *Electrochim Acta*, 2019, **318**: 901–910.
- [16] DU Y, KHAN S, ZHANG X, YU G, LIU R, ZHENG B, NADIMICHERLA R, WU D, FU R. In-situ preparation of porous carbon nanosheets loaded with metal chalcogenides for a superior oxygen evolution reaction[J]. *Carbon*, 2019, **149**: 144–151.
- [17] ZHAO D, SHAO Q, ZHANG Y, HUANG X. N-Doped carbon shelled bimetallic phosphates for efficient electrochemical overall water splitting[J]. *Nanoscale*, 2018, **10**(48): 22787–22791.
- [18] SINGH R N, SINGH J P, SINGH A. Electrocatalytic properties of new spinel-type MMoO_4 ($M = \text{Fe, Co and Ni}$) electrodes for oxygen evolution in alkaline solutions[J]. *Int J Hydrog Energy*, 2008, **33**(16): 4260–4264.
- [19] MAY K J, CARLTON C E, STOERZINGER K A, RISCH M, SUNTIVICH J, LEE Y L, GRIMAUD A, SHAO-HORN Y. Influence of oxygen evolution during water oxidation on the surface of perovskite oxide catalysts[J]. *J Phys Chem Lett*, 2012, **3**(22): 3264–3270.
- [20] FRIEBEL D, LOUIE M W, BAJDICH M, SANWALD K E, CAI Y, WISE A M, CHENG M J, SOKARAS D, WENG T C, ALONSO-MORI R, DAVIS R C, BARGER J R, NØRSKOV J K, NILSSON A, BELL A T. Identification of highly active Fe sites in $(\text{Ni, Fe})\text{OOH}$ for electrocatalytic water splitting[J]. *J Am Chem Soc*, 2015, **137**(3): 1305–1313.
- [21] KLAUS S, CAI Y, LOUIE M W, TROTOCHAUD L, BELL A T. Effects of Fe electrolyte impurities on $\text{Ni}(\text{OH})_2/\text{NiOOH}$ structure and oxygen evolution activity[J]. *J Phys Chem C*, 2015, **119**(13): 7243–7254.
- [22] LYU P, NATCHTIGALL P. Systematic computational investigation of an Ni_3Fe catalyst for the OER[J]. *Catal Today*, 2020, **345**: 220–226.
- [23] MA Y, DAI X, LIU M, YONG J, QIAO H, JIN A, LI Z, HUANG X, WWANG H, ZHANG X. Strongly coupled FeNi

- alloys/NiFe₂O₄@carbonitride layers-assembled microboxes for enhanced oxygen evolution reaction[J]. *ACS Appl Mater Interfaces*, 2016, **8**(50): 34396–34404.
- [24] LI W, HU Q, LIU Y, ZHANG M, WANG J, HAN X, ZHONG C, HU W, DENG Y. Powder metallurgy synthesis of porous Ni-Fe alloy for oxygen evolution reaction and overall water splitting[J]. *J Mater Sci Technol*, 2019, **37**: 154–160.
- [25] ULLAL Y, HEGDE A C. Electrodeposition and electro-catalytic study of nanocrystalline Ni-Fe alloy[J]. *Int J Hydrog Energy*, 2014, **39**: 10485–10492.
- [26] HOU Y, CUI S M, WEN Z H, GUO X R, FENG X L, CHRN J H. Strongly coupled 3D hybrids of N-doped porous carbon Nanosheet/CoNi alloy-encapsulated carbon nanotubes for enhanced electrocatalysis[J]. *Small*, 2015, **11**(44): 5940–5948.
- [27] SHAH S A, JI Z, SHEN X, YUE X, ZHU G, XU K, YUAN A, ULLAH N, ZHU J, SONG P, LI X. Thermal synthesis of FeNi@nitrogen-doped graphene dispersed on nitrogen-doped carbon matrix as an excellent electrocatalyst for oxygen evolution reaction[J]. *ACS Appl Energy Mater*, 2019, **2**(6): 4075–4083.
- [28] WANG C, SUI Y, XU M, LIU C, XIAO G, ZOU B. Synthesis of Ni-Ir nanocages with improved electrocatalytic performance for the oxygen evolution reaction[J]. *ACS Sustainable Chem Eng*, 2017, **5**(11): 9787–9792.
- [29] XIANG D, BO X, GAO X, ZHANG C, DU C, ZHENG F, ZHUANG Z, LI P, ZHU L, CHEN W. Novel one-step synthesis of core@shell iron-nickel alloy nanoparticles coated by carbon layers for efficient oxygen evolution reaction electrocatalysis[J]. *J Power Sources*, 2019, **438**: 226988.
- [30] LIU P S, LIANG K M. Preparation and corresponding structure of nickel foam[J]. *Mater Sci Technol*, 2000, **16**: 575–578.
- [31] JIN J, XIA J, QIAN X, WU T, LING H, HU A, LI M, HANG T. Exceptional electrocatalytic oxygen evolution efficiency and stability from electrodeposited NiFe alloy on Ni foam[J]. *Electrochim Acta*, 2019, **299**: 567–574.

Ni-Fe 合金泡沫的制备及电解水析氧性能研究

杨肖萌¹, 李作鹏^{1,*}, 秦君¹, 武美霞¹, 刘佳丽¹, 郭永¹, 马彦青^{2,*}, 冯锋^{1,*}

(1. 山西大同大学化学与化工学院, 山西 大同 037009; 2. 天津大学纳米颗粒和纳米系统国际研究中心, 天津 300072)

摘要: NiFe 羟基氧化物及其氢氧化物是一种有效的、含量丰富的且廉价的析氧反应催化剂。然而, 这类催化剂有着不可避免的缺陷—易脱落, 严重影响了它的长期稳定性, 因而阻碍了其工业应用; 同时, 导电性不高导致了其在析氧反应时较高的过电位。本文采用共电沉积法和模板去除法, 利用聚氨酯海绵作为模板, 电沉积了不同 Fe 含量的 NiFe 合金泡沫用于催化析氧反应, 并通过扫描电子显微镜 (SEM)、能谱仪 (EDS) 和 X 射线衍射仪 (XRD) 分别表征了 NiFe 合金泡沫的物理性质, 表明催化剂中 Ni 和 Fe 元素的存在及其分布均匀, 形成了多孔 NiFe 合金。通过循环伏安法 (CV)、线性扫描伏安法 (LSV)、电化学阻抗谱法 (EIS)、*I-t* 等测试了其 OER 性能。含铁量为 30% 的 NiFe 合金泡沫在过电位为 292 mV 即可产生 10 mA/cm² 的电流密度, Tafel 斜率为 126.12 mV/decade, 且具有良好的长期稳定性。由于没有任何复杂的电极制备方法和黏合剂, 本文所研究的 NiFe 合金泡沫非常适用于作为工业碱性介质中电解水的阳极材料。

关键词: 析氧反应; NiFe 合金泡沫; 多孔结构; 电解水

中图分类号: O643.36; TQ116.2

文献标识码: A